*geologica*acta

Volcanic sequence in Late Triassic – Jurassic siliciclastic and evaporitic rocks from Galeana, NE Mexico

E.M. CRUZ-GÁMEZ[1]   **F. VELASCO-TAPIA**[1]   **J.A. RAMÍREZ-FERNÁNDEZ**[1]   **U. JENCHEN**[1]   **P. RODRÍGUEZ-SAAVEDRA**[1]
A.A. RODRÍGUEZ-DÍAZ[2]   **A. IRIONDO**[3]

[1]Universidad Autónoma de Nuevo León, Facultad de Ciencias de la Tierra
Ex – Hacienda de Guadalupe, Carretera Linares – Cerro Prieto km. 8, Linares, Nuevo León
67700, México. Cruz-Gámez E-mail: esther.cruzgm@uanl.edu.mx

[2]Universidad Nacional Autónoma de México, Instituto de Geofísica
Ciudad Universitaria, Delegación Coyoacán, Ciudad de México, Distrito Federal 04510, México

[3]Universidad Nacional Autónoma de México, Centro de Geociencias
Blvd. Juriquilla No. 3001, Querétaro, Querétaro 76230, México

─┤ **A B S T R A C T** ├─

In northeastern Mexico, volcanic rocks interbedded with Late Triassic–Jurassic siliciclastic and evaporitic strata have been linked to magmatic arcs developed in the Pangea western margin during its initial phase of fragmentation. This work provides new petrographic and geochemical data for volcanism included in the El Alamar and Minas Viejas formations outcropping in the Galeana region. Andesitic dykes and sills (n= 10) in the El Alamar redbeds show SiO_2= 47.5–59.1% and MgO= 1.2–4.2%, as well as a geochemical affinity to island arc magmas. This work represents the first report of this tectonic setting in the region. Geological and petrographic evidence suggest that this arc system likely developed after ~220 and before ~193Ma. Trachy-andesitic and rhyodacitic domes (n= 20) associated with the Minas Viejas gypsum-carbonates sequence show SiO_2= 61.8–82.7% and MgO= 0.1–4.0% with a tectonic affinity to continental arc. A rhyodacite sample from this region has been dated by U-Pb in zircon, yielding an age of 149.4 ± 1.2Ma (n= 21), being the youngest age related to this arc. Finally, we propose a three-step model to explain the tectonic evolution from Late Triassic island arc to Jurassic continental arc system in the northeastern Mexico.

KEYWORDS | **Northeastern Mexico. Island arc. Continental arc. Late Triassic. Jurassic.**

INTRODUCTION

The tectonics of northeastern Mexico during Late Triassic–Jurassic was dominated by the opening of the Gulf of Mexico (Stern and Dickinson, 2010; Pindell and Horn, 2014). However, the mechanism responsible for such process remains controversial. A mantle plume (Dalziel *et al.*, 2000) or an upper mantle instability (related to thermal blanketing; Gurnis, 1988) have been suggested as causes of active rifting. In contrast, a far-field stresses due to trench retreat along the western continental margin has also been suggested as a passive driver of rifting (Gutiérrez-Alonso *et al.*, 2008).

Rifting was accompanied by the deposition of red beds sequences along the continental margins (Salvador, 1991; Goldhammer, 1999). These siliciclastic rocks (continental-facies red-colored sandstone, siltstone, shale, conglomerate

and mudstone) have been classified into several lithostratigraphic units (Barboza-Gudiño *et al.*, 2010): i) El Alamar Fm. (Late Triassic), mainly outcropping in the Galeana region, and incomplete sections in the Huizachal-Peregrina Anticlinorium; ii) Zacatecas Fm. (Late Triassic), whose exposures are distributed in the Mesa Central province (San Luis Potosí); iii) La Boca Fm. (Early to Middle Jurassic), exposed in the eroded core of the Huizachal-Peregrina Anticlinorium and Aramberri region; iv) Nazas Fm. (Early to Middle Jurassic), outcropping in the northeastern Mesa Central province (San Luis Potosí); and v) La Joya Fm. (Middle Jurassic), with exposures in all localities previously mentioned.

Extensive evaporitic sulphate successions including carbonate layers were deposited over the red beds during Callovian–Oxfordian times in the Huizachal-Peregrina Anticlinorium, Aramberri, and Galeana areas, and are termed the Minas Viejas or Olvido Fm. (Fig. 1; Goldhammer, 1999). Kroeger and Stinnesbeck (2003) suggested that these salt deposits represented the first evidence of the marine incursion into Northeastern Mexico.
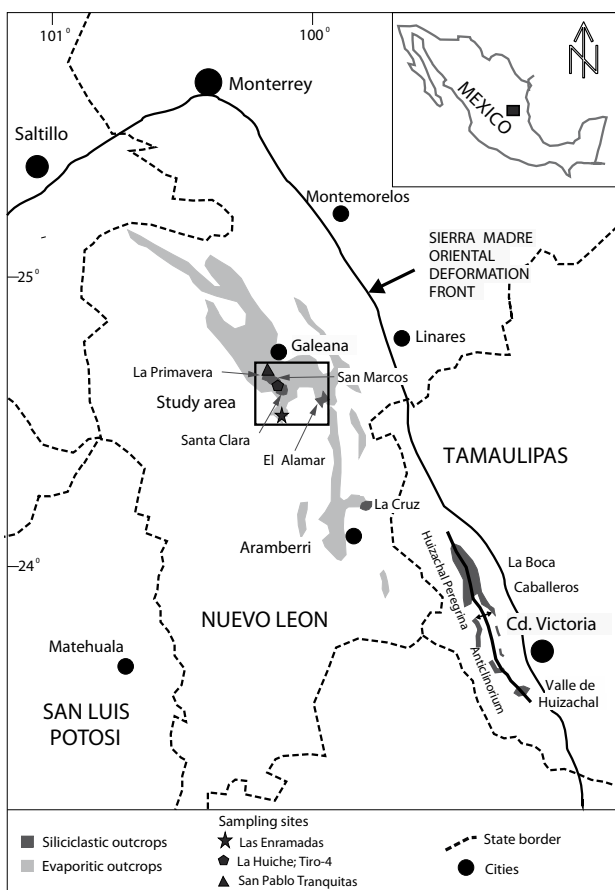
FIGURE 1. Distribution of the Early Mesozoic siliciclastic and evaporitic exposures in the Northeastern Mexico (modified after Padilla y Sanchez, 1985; Barboza-Gudiño *et al., 2*010), and location of the study area (black square).

Additionally, a magmatic arc was active from Permian through Jurassic times along the border between the northern (Laurentia) and southern (Gondwana) continental landmasses of Pangea (Torres *et al.*, 1999; Dickinson and Lawton, 2001). Stern and Dickinson (2010) reported that the Permian–Triassic East Mexico arc was active prior to Pangea break-up, whereas the Jurassic Nazas arc was coeval with the continental fragmentation process and the opening of the Gulf of Mexico. However, volcanic and intrusive rocks produced by these arcs are not well exposed. Felsic plutons linked to Permian–Triassic arc have been reported in the Coahuila, Tampico, and Yucatan-Chiapas blocks (Torres *et al.*, 1999; Dickinson and Lawton, 2001; Iriondo and Arvizu, 2009). Bartolini *et al.* (1999) reported volcanic rocks exposed in the following localities: La Cruz, Aramberri, in Nuevo León; Huizachal, Caballeros, and La Boca Canyons, and Miquihuana, in Tamaulipas; and Real de Catorce, in San Luis Potosí. These extrusive rocks are considered remnants of the Permian-Triassic arc. However, based on U-Pb in zircon dating, Barboza-Gudiño *et al.* (2008) suggested a Lower Jurassic age for the volcanism previously studied by Bartolini *et al.* (1999).

On the other hand, volcanic rocks associated with the Nazas arc have been reported in the Late Triassic–Middle Jurassic siliciclastic sequences (Jones *et al.*, 1995; Fastovsky *et al.*, 2005; Barboza-Gudiño *et al.*, 2010; Rubio-Cisneros *et al.*, 2011), and in the Late Jurassic evaporitic strata (Kroeger and Stinnesbeck, 2003; Cross, 2012). A general scheme (based on geologic and geochronologic data) about the relative position of volcanism included in the Triassic to Jurassic sedimentary units exposed in Galeana, Aramberri, and Ciudad Victoria (Huizachal-Peregrina Anticlinorium) is shown in Figure 2.

The purpose of this paper is to provide new petrographic and geochemical data on the volcanic rocks included in the El Alamar (red beds) and Minas Viejas (gypsum-carbonate sequences) units from the Galeana region (Fig. 1). This information, interpreted in an appropriate geological framework, is used to construct a conceptual model explaining the origin and tectonic affinity of the Late Triassic to Jurassic volcanism, and its implications for the geological evolution of northeastern Mexico.

GEOLOGICAL SETTING

The Mesozoic sedimentary units of the Sierra Madre Oriental were deposited on heterogeneous Precambrian–Paleozoic crystalline basement. Siliciclastic units (El Alamar, La Boca and La Joya) represent the first stratigraphic record, covering the Late Triassic to Middle Jurassic period (Fig. 1).
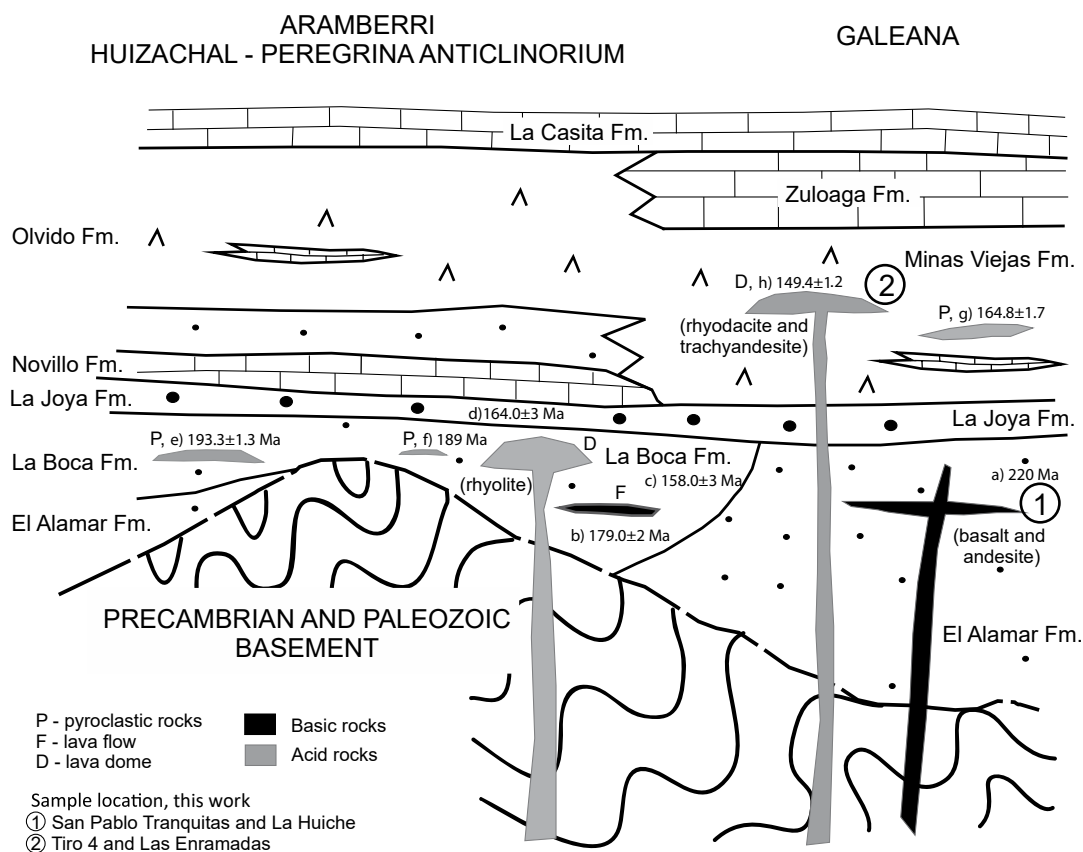
FIGURE 2. Generalized stratigraphic scheme for the Early Mesozoic sedimentary and volcanic rocks included in the Galeana, Arramberri and Valle de Huizachal localities (based on Barboza-Gudiño *et al.,* 2008, 2014). U-Pb ages for siliciclastic and pyroclastic rocks: a) El Alamar Fm. - San Marcos (detrital zircon), Barboza-Gudiño *et al.* (2014): 220Ma; b) Lower La Boca Fm. - Valle de Huizachal (detrital zircon), Rubio-Cisneros (2012): 179.0 ± 2.0Ma; c) Upper La Boca Fm. - Valle de Huizachal (detrital zircon), Rubio-Cisneros (2012): 158.0 ± 3.0Ma; d) La Joya Fm. - Valle de Huizachal (detrital zircon), Rubio-Cisneros (2012): 164.0 ± 3.0Ma; e) La Boca Fm. - Arramberri (tuff), Barboza-Gudiño *et al.* (2008): 193.3 ± 1.3Ma; f) La Boca Fm. - Valle de Huizachal (tuff), Fastovsky *et al.* (2005): 189Ma; g) Minas Viejas Fm. - La Primavera (tuff), Cross (2012): 164.8 ± 1.7Ma; h) Minas Vieja Fm. - Tiro-4 (dome), this work: 149.4 ± 1.2Ma. See Figure 1 for sample location.

The Late Triassic El Alamar Fm. is the oldest unit of the local stratigraphy, and was deposited in an extensional basin located in the Galeana region (Barboza-Gudiño *et al.*, 2010). This unit (thickness ~350m) is composed of sandstone, claystone, siltstone, and conglomerate deposited in an alluvial to lacustrine setting. Petrified wood fragments are common in sandy and conglomeratic beds. Best-preserved outcrops of this unit are located in the San Marcos and El Alamar areas (Fig. 1). It is important to note that the El Alamar Fm. is cut by gray-green basic to intermediate porphyritic dykes and sills (Fig. 3A, C; La Huiche mine and San Pablo Tranquitas localities; thickness: 3–7m).

In the Galeana area, the El Alamar Fm. is overlain along an angular unconformity by the Middle Jurassic La Joya Fm., composed of sandstone and conglomerate without evidence of interbedded volcanic rocks. Reworked volcanic clasts are observed in the conglomerate (Fig. 3D). The El Alamar and La Joya units are overlain by the Late Jurassic Minas Viejas Fm., whose outcrops are well exposed in this region (Fig. 1). According to Kroeger and Stinnesbeck (2003), this lithostratigraphic unit is divided into the Las Minas member, a sequence of limestone interbedded with gypsum, and the La Primavera member, which is composed of terrigenous sediments and gray to reddish felsic pyroclastic rocks interbedded with gypsum. Additionally, in the Tiro 4 (Huiche mine) and Las Enramadas outcrops cream to reddish colored felsic dome structures (diameter: 3–4m and 350m respectively; Fig. 3E, F) cut the gypsum and carbonate sequence. Las Enramadas outcrop also displays flow, aphyric and breccia structures.

METHODOLOGY

Volcanic rocks were sampled in the La Huiche, San Pablo Tranquitas, Tiro 4 and Las Enramadas outcrops (12 samples; ~2.5kg/sample) (Fig. 2; Table 1).
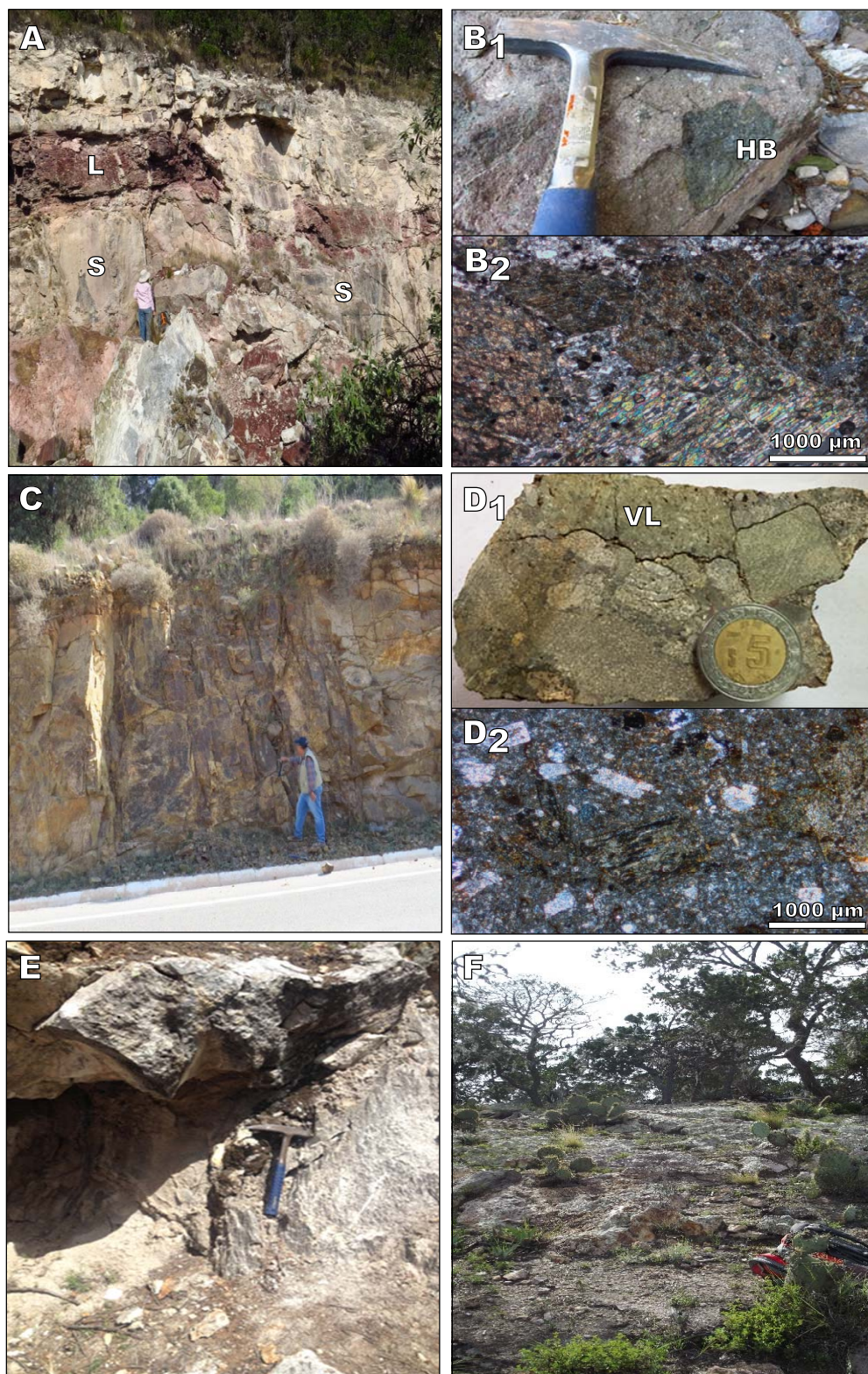
FIGURE 3. Volcanic rocks included in the El Alamar and Minas Viejas fms., Galeana area (see Figure 1 for sampling sites): A) Andesitic sill (S) in the El Alamar limolite (L), affected by normal faulting with lateral component, from La Huiche locality. The faults displace the strata as well as the sills vertically a maximum of ~2m; B1) Hornblenditic enclave (HB) in andesitic sill from La Huiche locality; B2) Photomicrograph of magmatic enclave containing euhedral hornblende; C) Andesitic dyke in the upper section of the El Alamar Formation from San Pablo Tranquitas locality; D1) La Joya conglomerate, from San Pablo Tranquitas locality, showing volcanic lithoclasts (VL); D2) Photomicrograph of the volcanic lithoclast (showed in D1), constituted by a porphyric andesite; E) Rhyodacite cutting the evaporitic Minas Viejas sequence (Tiro-4, La Huiche mine); F) Trachyandesitic dome from Las Enramadas locality, showing a lava flow structure.

TABLE 1. Petrographic data of representative Late Triassic–Jurassic volcanic rocks of Galeana area

Sample	Qz	Pl	Pl^{alt}	Amp	Amp^{alt}	Fsp	Ol	Ep	Chl	Ser	Cal	Brt	Glass	Op	Zrn
						La Huiche									
LH-10-05	6.0		51.0		26.0				3.0	4.5	6.5	1.0		2.0	
LH-10-06		10.0	54.0		16.0				3.3	4.0	4.7	0.5	6.5	1.0	
SN-1	1.0		53.0		25.0		3.0		5.0	5.0	7.0			0.5	0.5
H-M1	2.0		60.0		19.0				3.0	4.2	2.0	1.0	7.0	1.8	
HUI-4		40.0	10.0	18.0	10.0			7.0	5.5	4.0	3.3			1.5	0.7
HUI-9			52.0		28.0				5.0	6.0	8.0			0.5	0.5
HUI-10		17.0	38.0	15.0	15.5			2.0	4.0	3.0	2.5			3	
					Tiro 4 (La Huiche mine)										
TIRO 4-1	21.0	37.0			21.0							2.7	17.0	1.0	0.3
TIRO 4-3	23.0	31.0			23.0						2.3	3.0	15.0	2.5	0.2
TIRO 4-4	22.0	30.0			23.0						5.0	2.8	17.0	0.1	0.1
TIRO 4-10	21.0	34.0			25.0						5.8		13.0	1.0	0.2
TIRO 4-11	35.0	26.0			21.0							1.9	15.5	0.5	0.1
					San Pablo Tranquitas										
SP-01			63.0		19.0				4.0	3.0	4.5		5.5	0.7	0.3
					Las Enramadas										
ENR-03	2.0	72.0			22.8									3.2	
ENR-06	2.0	71.0			22.4									4.6	
ENR-01	3.0	69.0			23.0									5.0	
ENR-1a	3.0	72.0			23.0									2.0	
ENR-2a	2.0	69.0			22.5									6.5	
ENR-3a	5.0	70.0			22.0									3.0	

Location of each profile can be found in Figure 1. Abbreviations for names of rock-forming minerals (Whitney and Evans, 2010): Qz: quartz, Pl: plagioclase, Pl^{alt}: plagioclase altered to sericite, Amp: amphibole, Amp^{alt}: amphibole altered to chlorite and calcite, Fsp: K-feldspar, Ol: olivine, Ep: epidote, Chl: chlorite, Ser: sericite, Cal: calcite, Brt: barite, Op: opaque, Zrn: zircon. All contents reported as %.

Modal compositions were determined by point counting on thin sections using a Leica petrographic microscope. Approximately 550 points per sample were counted in order to obtain a representative mode (Table 1).

Rock samples were jaw crushed and splits were pulverized in an agate bowl obtaining a 400-mesh fine powder. Major and trace element analysis were performed in Bureau Veritas Commodities Ltd. (Vancouver, Canada) laboratories by the LF200 methodology (Table 2). Each sample was fused using lithium borate and the melt produced was completely dissolved with hot Aqua Regia. Major and trace (Ba, Ni, Sc, Y and Zr) elements were analyzed in the resulting solution by inductively coupled plasma-optical emission spectrometry (ICP-OES detection limit: major elements ~0.01%; trace elements= 0.1–5.0ppm). The remaining trace elements, including Rare Earth Elements (REE), were determined by inductively coupled plasma–mass spectrometry (ICP-MS detection limits= 0.05–0.5ppm).

New petrographic (Table 1) and geochemical (major and trace elements; Table 2) data on the volcanic rocks from Galeana were compiled in a Statistical for Windows 5.0 database. Information previously reported by Bartolini *et al.* (1999), Barboza-Gudiño *et al.* (2008) and Rubio-Cisneros (2012) was also incorporated in this catalogue. Thus, the database are constituted by 32 volcanic samples from the El Alamar, La Boca, and Minas Viejas fms. Immobile geochemical ratios were used to establish the lithological classification. Furthermore, several normalized and variation diagrams were constructed to infer the geochemical features, origin, and tectonic setting for the Galeana volcanism.

Zircon mineral separation for the rhyodacite TIRO-4 (~1–2kg) was produced at the Mineral Separation and Characterization Laboratory (SEPCAMLab), Centro de Geociencias at Universidad Nacional Autónoma de México, using conventional methods (crushing, sieving, magnetic separation, and heavy liquids). Zircons for U-Pb geochronology were mounted in epoxy and grounded to nearly half their thickness using abrasives. Transmitted- and reflected-light photos (not shown) were taken of all mounted grains to aid in the spot selection to perform the laser ablation ICP-MS studies. In addition, scanning electron microscope-cathodoluminescence images (SEM-CL) of all zircons were obtained at the SEPCAMLab and used to reveal internal zoning related to chemical composition variations in order to avoid possible problematic areas within grains.

U-Th-Pb zircon geochronology of the rhyodacite sample was conducted in the Laboratorio de Estudios Isotópicos (LEI), Centro de Geociencias at Universidad Nacional Autónoma de México, using a Resonetics Workstation model M050 equipped with a LPX220 excimer laser coupled with a Thermo ICap Qc quadrupole ICP-MS (inductively coupled plasma–mass spectrometer) following analytical techniques similar to those reported by Solari *et al.* (2010) and González-León *et al.* (2016). Sample spot beam locations are ~23μm in diameter. To account for down-hole fractionation observed in the primary standard zircon, the data reduction was performed using the comercial software "Iolite 2.5" (Paton *et al.*, 2010, 2011), employing the VizualAge data reduction scheme presented in Petrus and Kamber (2012). The primary zircon-bracketing standard used was 91500

TABLE 2. Major (% wt) and trace element (ppm) compositions of volcanic rocks of Galeana area

Sample	TIRO 4-3	TIRO 4-4	LH-10-06	LH-10-05	SN-1	SP-01	ENR-03	ENR-06	ENR-01	ENR-1a	ENR-2a	ENR-3a	SO-19f[c]	SO-19e[c]
Coordinate N	2728900	2728900	2728989	2728989	2728983	2731184	2721989	2721989	2721989	2721929	2721929	2721929		
Coordinate E	14R390325	14R390325	14R390236	14R390236	14R390260	14R389605	14R389236	14R389236	14R389236	14R389351	14R389351	14R389351		
Locality	Tiro 4	Tiro 4	La Huiche	La Huiche	La Huiche	San Pablo	Enramadas	Enramadas	Enramadas	Enramadas	Enramadas	Enramadas		
Rock Type	Rhyodacite	Rhyodacite	Andesite	Andesite	Andesite	Andesite	Trachyandesite	Trachyandesite	Trachyandesite	Trachyandesite	Trachyandesite	Trachyandesite	Trachyandesite	Trachyandesite
SiO_2	49.06	52.28	46.75	48.43	45.49	50.10	71.99	70.00	68.91	75.53	69.22	99.20	60.21	61.13
TiO_2	0.32	0.41	0.95	0.85	0.86	0.75	0.52	0.50	0.45	0.67	0.47	0.57	0.71	0.69
Al_2O_3	12.39	13.76	18.89	17.24	17.44	18.31	16.29	16.41	15.46	14.14	17.23	13.35	14.04	13.95
$Fe_2O_3^t$	2.67	0.86	8.50	11.54	9.55	7.85	0.75	2.38	3.72	0.20	5.84	0.97	7.57	7.47
MnO	0.01	0.02	0.16	0.26	0.26	0.16	0.01	0.01	0.01	0.02	0.02	0.05	0.13	0.13
MgO	0.07	0.16	2.97	3.74	3.53	2.62	0.03	0.05	0.03	0.02	0.02	0.29	2.88	2.88
CaO	0.72	6.23	6.80	6.57	6.57	5.93	0.10	0.14	0.13	0.21	0.43	0.43	6.00	6.00
Na_2O	7.12	7.84	5.89	2.16	2.64	4.03	9.24	9.08	8.30	7.31	9.89	9.89	4.05	4.05
K_2O	0.04	0.05	1.25	2.39	2.92	2.39	0.11	0.07	0.08	0.09	0.07	0.15	4.11	4.11
P_2O_5	0.03	0.14	0.19	0.19	0.21	0.21	0.07	0.07	0.08	0.06	0.15	0.15	1.29	1.29
LOI	2.60	5.70	7.40	10.10	10.30	7.40	0.80	1.20	2.70	0.80	0.80	4.20	0.32	0.32
Sum	99.03[a]	99.85[a]	99.75	99.74	99.77	99.75	99.91	99.92	99.90	99.28	101.18	99.25	99.11	99.11
CO_2	0.02	4.26	4.73	5.61	5.64	4.10	0.04			0.01	0.08	0.08		
Sc	2	5	26	24	22	17	4	4	4	4			29	27
V	19	68	276	243	237	171	36	78	45	83	63	69	174	165
Co	11		19	29	16.4	14.9		1.0			1.0	2.0	24.8	24.0
Ni	6.0	1.0	7.0	25	4.2	3.8	1.0				1.0	17.0	24.0	470
Zn	2		90	92	30	65						19	462	470
Ga	7.0	11.0	19.0	19.0	17.7	18.6	18.0	18.0	17.0	18.0	19.6	19	17.5	17.0
Rb	1	1	35	59	82	58	2	1	1	1	4	7	20	20
Sr	3300	2050	488	132	240	240	352	277	414	102	343	72	340	317
Y	5	11	19	17	72	22	7	6	8	9	10	14	34.8	35.5
Zr	82	105	81	100	73	107	165	152	145	207	164	158	112	112
Nb	2.6	3.1	3.4	4.1	2.9	4.5	6.2	5.8	5.2	7.0	5.9	6.0	68.5	68.5
Cs		0.1	1.8	9.0	2.3	3.5		0.4	0.1	0.5	0.3	0.5	4.2	4.5
Ba	24.0[b]	12.4[b]	174	515	700	643	40	47	70	28	23	78	498	486
La	5.7	13.1	28.8	45.7	21.1	28.0	10.3	5.1	9.9	11.1	21.0	12.0	69.5	71.3
Ce	0.66	22.8	56.3	93.7	42.6	59.9	20.5	12.5	16.3	24.4	43.3	15.6	156.5	161.0
Pr	2.4	2.68	6.57	10.37	5.15	6.67	2.444	1.46	2.37	2.93	5.79	2.76	18.97	19.40
Nd	0.42	10.0	25.2	37.2	21.6	25.5	10.8	5.8	9.2	11.4	25.5	11.0	73.9	75.7
Sm	2.15	2.41	4.76	5.24	4.66	5.09	1.89	1.17	1.19	2.26	4.46	2.60	12.71	13.70
Eu	0.10	3.34	1.37	1.18	1.38	1.55	0.35	0.37	0.40	0.56	1.30	0.58	3.45	3.81
Gd	0.61	0.33	4.53	4.18	4.07	5.37	1.28	1.18	1.59	1.69	3.72	2.36	9.92	10.53
Tb	0.13	1.85	0.63	0.55	0.58	0.77	0.17	0.19	0.26	0.24	0.46	0.39	1.28	1.41
Dy	0.49	0.4	3.57	2.94	3.16	4.39	1.10	1.13	1.50	1.43	1.85	2.34	6.94	7.50
Ho	0.13	1.97	0.75	0.61	0.60	0.84	0.23	0.24	0.31	0.30	0.46	0.46	1.32	1.39
Er	0.83	0.20	1.97	1.79	1.88	2.24	0.99	0.88	1.06	0.90	1.09	1.41	3.35	3.78
Tm	0.17	1.53	0.31	0.25	0.27	0.36	0.14	0.12	0.15	0.16	0.17	0.19	0.51	0.55
Yb		0.26	1.96	1.81	1.78	2.29	1.19	0.96	1.09	1.09	1.09	1.45	3.19	3.55
Lu			0.29	0.29	0.26	0.30	0.20	0.14	0.17	0.18	0.18	0.22	0.49	0.53
Hf	2.5	2.7	2.3	2.5	2.1	2.8	4.4	3.8	3.6	5.4	4.4	4.2	2.9	3.1
Ta	0.6	0.4	0.3	0.4	0.2	0.3	0.4	0.4	0.3	0.4	0.6	0.4	4.2	4.9
Pb	1.0	5.5	6.7	10.4	6.1	9.4	1.0		1.0	1.0	3.1	1.8	13.8	13.0
Th	5.7	1.5	2.2	2.6	2.0	2.6	3.6	3.1	3.2	4.0	3.2	3.7	20.2	19.4
U	1.7						3.0	5.1	1.7	3.6	6.7	0.8		

[a] Major element sum in addition to %BaSO4 (barite).
[b] %BaSO4 determined by gravimetric method.
[c] Veritas internal reference material; t= theoretical data, e= experimental data.

(Wiedenbeck *et al.*, 1995; TIMS age of 1065.4 ± 0.6Ma) whereas Plešovice standard (Plešovice; Slama *et al.*, 2008; TIMS age of 337.13 ± 0.37Ma) was used as secondary standard control. All uncertainties were propagated using Iolite protocols and are reported at 2-sigma level of precision (Table 3). The data were exported from Iolite and plotted with computational software "Isoplot 3.0" (Ludwig, 2003) and shown in Concordia diagrams and a weighted mean age plot. No common Pb correction was applied to the geochronology data because the ^{204}Pb signal is insignificant in comparison to the overwhelming ^{204}Hg signal present in our system.

RESULTS

Basic and intermediate rocks

Fieldwork reveals that Triassic to Jurassic continental deposits in the Galeana area (San Marcos, El Alamar and Santa Clara localities; Fig. 1) include basic to intermediate dykes and sills (Fig. 3A, C). These rocks display a porphyritic texture, with amphibole (longitude≤ 5cm; Fig. 4A, B) and plagioclase (longitude ~2–3cm) phenocrysts accompanied by an aphanitic groundmass of altered glass and plagioclase microcrystals (Fig. 4A; Table 1). However, some samples show a grain-size graded texture, with a similar mineral arrangement, characterized by a crystalline matrix (Fig. 4B; Table 1). Both rock types also contain olivine pseudomorphs, zircons, and opaque minerals (diameter<0.5cm), as well as propylitic alteration phases (sericite, chlorite, calcite, and epidote probably derived from amphibole and plagioclase; as well as quartz, calcite, and barite in veins).

It is important to note that the intermediate rocks include uncommon centimeter size hornblende enclaves (*e.g.* coarse grained cumulus mineral phases; Fig. 3B1, B2), and a similar texture and mineralogical arrangements to those observed in the La Joya reworked volcanic clasts (Fig. 3D1, D2).

Basic and intermediate rocks (n= 10) are characterized by SiO$_2$= 47.5–59.1% and MgO= 1.2–4.2% expressed as adjusted data in an anhydrous base (original data reported in Table 2).

Acid rocks

Dome structures with an acid composition have been observed in the Minas Viejas Fm. (Tiro-4 and Las Enramadas localities; Fig. 1). These rocks show porphyritic or trachytic texture. The former are mainly constituted by plagioclase and K-feldspar (longitude ~2cm), as well as quartz microcrystals, embedded in a fine grained matrix of the same minerals and glass (Fig. 4C; Table 1). Mineralogical paragenesis is completed by zircon and opaque microcrystals, in addition to calcite, barite and quartz veins (Fig. 4D). Trachytic texture rocks are conformed by plagioclase laths (longitude ~0.3cm), with subordinate quartz, K-feldspar, opaque minerals and sulphur oxide pseudomorphs (Fig. 4E, F; Table 1). Acid rocks (n= 20) display geochemical compositions of SiO$_2$= 61.8–82.7% and MgO= 0.1–4.0% expressed as adjusted data in an anhydrous base (original data reported in Table 2).

Forty zircon crystals were separated from the Tiro-4 sample (Table 3). Position of the LA-ICP-MS spots in zircon specimens were selected using SEM-CL images. These grains are characterized by U= 96.5–900ppm and Th= 42.1–877ppm, with a Th/U= 0.16–1.27. U-Pb isotopic information related to zircons, after the detection and elimination of outliers, in a Concordia diagram has revealed an age of 149.4 ± 1.2Ma (n= 21; MSWD [Mean Squares of Weighted Deviates]= 2.0).

DISCUSSION

Classification and geochemical general features

Petrography reveals pervasive alteration of the original phenocrysts and volcanic Galeana intermediate rocks (Fig. 4), probably related to interaction with hydrothermal fluids and weathering. In this scenario, major-elements and Large Ion Lithophile Elements (LILE) are not suitable to establish a geochemical classification and an inference about igneous processes.

However, during alteration High Field Strength Elements (HFSE) and REE are strongly retained in particulate material and not released by dissolution. For this reason, these immobile elements were used to establish a classification and tectonic-setting affinity of altered volcanic rocks. In fact, Zr/Ti and Nb/Y ratios (Fig. 5; Winchester and Floyd, 1977) reveal that the volcanism from Galeana (Figs. 1; 2) is distributed in two groups: i) andesitic dykes and sills in the El Alamar sequence and ii) acid rocks (trachyandesite, rhyodacite and rhyolite) that appear as lava dome and pyroclastic fragments in the Minas Viejas evaporites. Sub-alkaline basalt and andesite, as well as rhyodacite, rhyolite, and trachyandesite, are also intercalated in the La Boca outcrops from the Anticlinorium Huizachal Peregrina and Aramberri (Fig. 5; Bartolini *et al.*, 1999; Fastovsky *et al.*, 2005; Barboza-Gudiño *et al.*, 2008; Rubio-Cisneros, 2012).

Intermediate rocks show light-REE enriched chondrite-normalized patterns (Fig. 6A, C), showing [La/Yb]$_N$= 3.4–
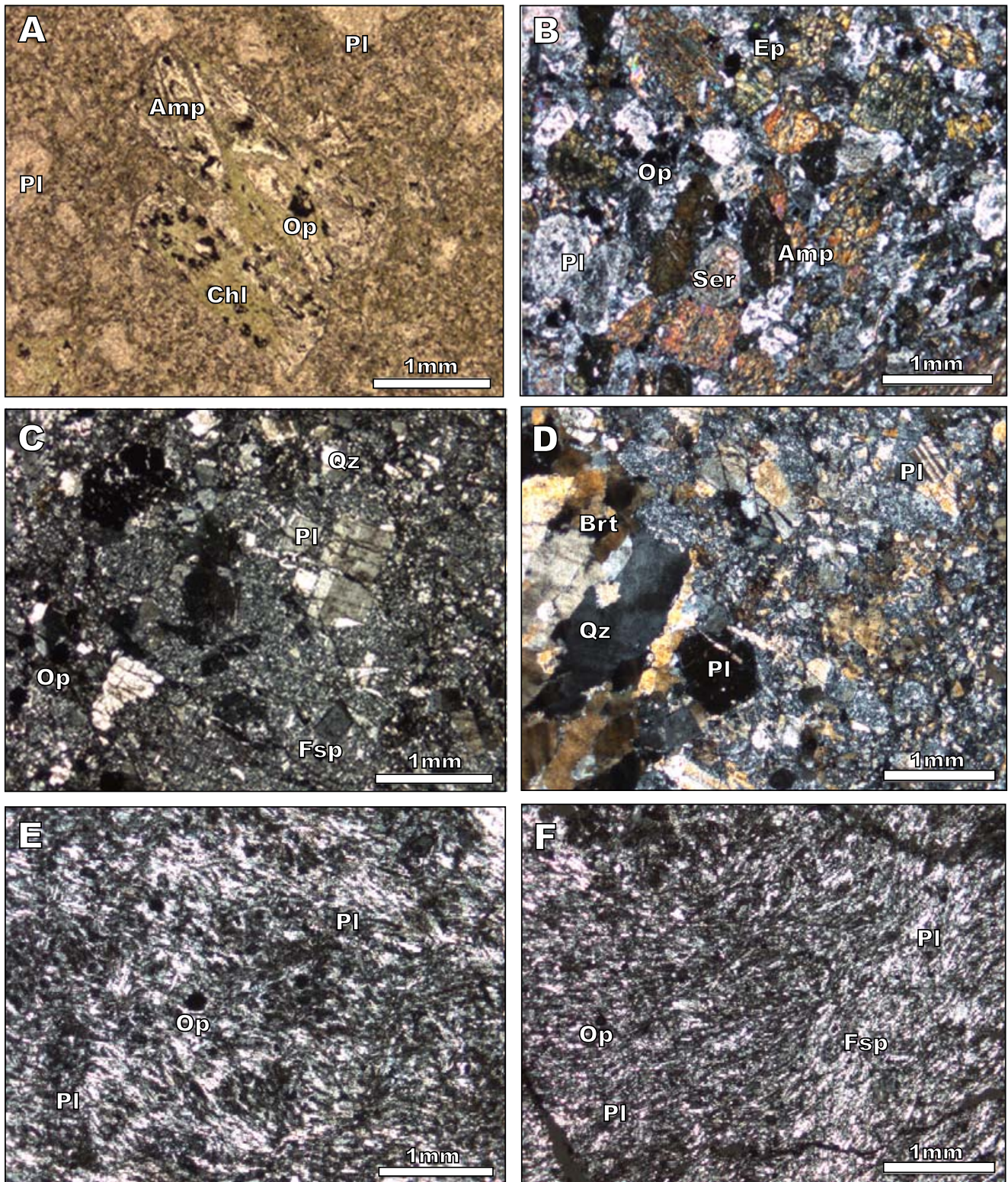
FIGURE 4. Photomicrographs for volcanic rocks included in the El Alamar and Minas Viejas fms., Galeana area: A) Porphyric andesite with chloritized amphibole phenocrysts and opaque minerals embedded in a microcrystalline groundmass (sample SP-01, 2.5x, NII; San Pablo Tranquitas); B) Highly altered andesite showing sericitized feldspar phenocrysts, epidote and abundant hypidiomorphic amphibole included in a grain-size graded matrix (sample Hui-10, 2.5x NX; La Huiche mine); C) Porphyric rhyodacite with feldspar and quartz in a microlite matrix (sample Tiro 4-3, 2.5x, NX; Tiro 4 - La Huiche mine); D) Quartz and barite vein in rhyodacite, showing inequigranular feldspar (sample Tiro 4-4, 2.5x, NX; Tiro 4 - La Huiche mine); E) Trachyandesite displaying oriented plagioclase crystals (trachyte texture) and sulphur pseudomorphs (sample ENR-04 2.5x, NX; Las Enramadas); F) Trachyandesite with oriented plagioclase microlites, K-feldspar and opaque minerals (sample ENR-01 2.5x, NX; Las Enramadas).

16.9 (n= 10), without evidence of negative Eu anomaly (quantified by Eu/Eu*= Eu_N/[Sm_N*Gd_N]1/2= 0.8–1.2), and a flat pattern for heavy-REE. Acid rocks display similar REE patterns (Fig. 6B, D; n= 16), with [La/Yb]$_N$= 3.5–14.6 and Eu/Eu*= 0.6–1.0.

Figures 7A-D show Mid-Ocean Ridge Basalt (MORB) normalized multi-element patterns for volcanic rocks. The most mobile elements (LILE: Sr, K, Rb, Ba) are located on the left organized in order of increasing incompatibility. The remaining elements are considered immobile and are arranged in order of increasing incompatibility from right to left. Intermediate rocks show a marked enrichment in LILE (reaching 50X of MORB) and small depletion of Nb-Ta and TiO$_2$ (Figs. 7A, C). Acid rocks from La Boca Fm. and sample RCII-21 from El Alamar (Rubio-Cisneros, 2012) display MORB-normalized multi-element patterns comparable to the intermediate group (Fig. 7D). In contrast, acid rocks collected in the Minas Viejas evaporites are characterized by zig-zag patterns with lower concentration in lithophile elements (K$_2$O-Rb-Ba being ~0.9-5.0X of

MORB) in comparison with the rest of Galeana volcanic lithologies (Fig. 7C).

Tectonic affinity

Discrimination diagrams widely used in the literature have been applied to determine the tectonic setting of the Galeana volcanism. The Ti-V diagram by Shervais (1982) and the Nb-Zr-Y diagram by Meschede (1986) (Fig. 8A, B) reveal that intermediate rocks display an affinity to an arc tectonic setting. In addition, these rocks are characterized by ratios of Th/La= 0.36 ± 0.21 (n= 10; range= 0.23–0.95). Plank (2005) reported a Th/La average ratio of 0.25 ± 0.07 (n= 215) for arc basalts. In the case the felsic rocks (Fig. 8C, D), a subduction tectonic setting has been also established using the Rb–(Y + Rb) diagram by Pearce *et al.* (1984) and the Th/Ta–Yb diagram by Gorton and Schandl (2000).

However, the tectonic discrimination efficiency of these conventional diagrams has been strongly

TABLE 3. U-Th-Pb analytical data for LA-ICPMS spot analyses on zircon grains for rhyodacite Tiro-4, Galeana area

Analysis	U^a ppm	Th^a ppm	Th/U	207Pb/206Pb	err%	207Pb/235U	err%	206Pb/238U	err%	208Pb/232Th	err%	Rho^d	%disc	206Pb/238U	±2s	207Pb/235U	±2s	207Pb/206Pb	±2s	Best age^e Ma	±	2s
Tiro4-23	187	62	0.33	0.06620	8.2	0.19600	7.1	0.02199	2.7	0.01175	6.2	0.376	23	140.2	3.8	181.0	12.0	769	99	140.2	±	3.8
Tiro4-10	272	159	0.59	0.05600	6.3	0.16840	6.5	0.02224	2.8	0.00784	4.7	0.434	10	141.8	3.9	157.5	9.5	472	64	141.8	±	3.9
Tiro4-18	689	877	1.27	0.05340	4.1	0.16500	4.8	0.02242	2.3	0.00698	3.4	0.478	8	142.9	3.3	154.9	6.9	355	68	142.9	±	3.3
Tiro4-28	251	136	0.54	0.05630	5.7	0.17870	6.2	0.02280	2.4	0.00859	4.5	0.392	13	145.3	3.4	167.8	10.0	569	88	145.3	±	3.4
Tiro4-09	449	292	0.65	0.05080	5.7	0.16170	5.7	0.02294	2.0	0.00745	3.6	0.360	4	146.2	3.0	151.9	8.0	291	54	146.2	±	3.0
Tiro4-31	253	108	0.42	0.06090	6.6	0.19700	7.1	0.02294	2.8	0.00966	5.9	0.399	20	146.2	4.1	182.0	12.0	695	98	146.2	±	4.1
Tiro4-29	288	187	0.65	0.05710	5.6	0.18100	6.0	0.02299	2.2	0.00784	4.6	0.328	14	146.5	3.2	169.4	11.0	530	82	146.5	±	3.2
Tiro4-33	349	224	0.64	0.05320	4.9	0.16880	5.9	0.02303	3.0	0.00768	3.8	0.498	7	146.7	4.3	158.0	9.0	363	66	146.7	±	4.3
Tiro4-04	303	135	0.45	0.05090	5.5	0.16150	5.4	0.02304	2.4	0.00743	5.0	0.438	3	146.8	3.5	151.8	7.7	296	71	146.8	±	3.5
Tiro4-16	284	330	1.16	0.04920	6.5	0.15620	7.0	0.02307	2.1	0.00746	3.5	0.302	0	147.0	3.1	147.0	9.3	310	71	147.0	±	3.1
Tiro4-32	211	78	0.37	0.05670	6.2	0.18200	7.1	0.02309	3.0	0.00871	6.9	0.418	13	147.2	4.3	169.0	11.0	536	88	147.2	±	4.3
Tiro4-25	534	331	0.62	0.05040	5.4	0.16140	5.4	0.02313	2.3	0.00786	5.1	0.433	3	147.4	3.4	151.7	7.6	241	49	147.4	±	3.4
Tiro4-20	270	108	0.40	0.05180	6.4	0.16790	6.0	0.02319	2.2	0.00731	5.1	0.362	6	147.8	3.1	157.2	8.9	355	66	147.8	±	3.1
Tiro4-34	227	132	0.58	0.05570	7.0	0.17800	7.9	0.02320	3.2	0.00757	5.3	0.411	11	147.8	4.7	167.0	12.0	497	84	147.8	±	4.7
Tiro4-03	264	120	0.45	0.05160	6.2	0.16600	6.6	0.02320	2.7	0.00778	5.0	0.410	5	147.9	4.0	155.5	9.2	399	87	147.9	±	4.0
Tiro4-26	218	80	0.37	0.05930	6.9	0.19000	6.8	0.02331	3.0	0.00865	5.9	0.433	16	148.5	4.3	176.1	11.0	531	91	148.5	±	4.3
Tiro4-11	221	81	0.36	0.05380	7.4	0.16800	7.7	0.02331	2.6	0.00723	6.1	0.333	7	148.6	3.8	159.0	11.0	473	85	148.6	±	3.8
Tiro4-07	298	142	0.48	0.05430	5.5	0.17260	5.8	0.02332	2.3	0.00783	4.9	0.400	8	148.6	3.4	161.3	9.0	434	79	148.6	±	3.4
Tiro4-40	217	73	0.34	0.05560	5.8	0.17680	5.6	0.02336	2.7	0.00969	6.2	0.489	10	148.8	4.1	166.2	8.2	488	65	148.8	±	4.1
Tiro4-14	284	159	0.56	0.05540	6.0	0.17900	7.3	0.02340	2.6	0.00817	4.4	0.359	11	149.1	3.8	168.0	10.0	433	69	149.1	±	3.8
Tiro4-08	272	157	0.58	0.05430	6.4	0.17500	6.9	0.02341	2.3	0.00784	4.2	0.330	9	149.1	3.3	163.5	10.0	394	61	149.2	±	3.3
Tiro4-37	268	174	0.65	0.05120	5.7	0.16920	5.9	0.02344	2.5	0.00785	3.9	0.498	6	149.4	4.3	159.6	8.7	325	66	149.4	±	4.3
Tiro4-22	350	241	0.69	0.05420	5.5	0.17430	5.7	0.02347	2.0	0.00784	4.1	0.356	9	149.5	3.0	163.9	8.9	422	71	149.5	±	3.0
Tiro4-24	275	148	0.54	0.05820	7.2	0.19300	7.3	0.02347	2.3	0.00914	4.5	0.311	16	149.5	3.3	179.0	12.0	594	85	149.5	±	3.3
Tiro4-12	218	93	0.43	0.05230	8.0	0.16500	7.3	0.02351	3.1	0.00820	6.2	0.427	3	149.8	4.6	154.7	11.0	471	75	149.8	±	4.6
Tiro4-13	320	151	0.47	0.05410	5.4	0.17600	5.7	0.02359	2.2	0.00746	5.2	0.395	9	150.3	3.4	164.3	8.7	346	58	150.3	±	3.4
Tiro4-15	307	155	0.50	0.05490	6.0	0.17750	6.2	0.02360	2.5	0.00807	4.5	0.397	9	150.3	3.7	165.5	9.9	414	80	150.3	±	3.7
Tiro4-39	283	123	0.44	0.05200	5.4	0.17530	6.3	0.02362	2.5	0.00827	5.2	0.398	9	150.5	3.7	164.7	9.4	364	67	150.5	±	3.7
Tiro4-01	192	95	0.50	0.05640	7.3	0.18200	7.1	0.02367	3.1	0.00874	5.9	0.432	11	150.8	4.6	168.9	11.0	522	100	150.8	±	4.6
Tiro4-21	241	105	0.44	0.05160	6.7	0.18100	7.2	0.02375	2.6	0.00897	5.7	0.363	10	151.3	3.9	167.9	11.0	515	81	151.3	±	3.9
Tiro4-05	291	168	0.58	0.05090	5.9	0.16850	5.9	0.02388	2.2	0.00788	4.7	0.374	4	152.1	3.4	157.7	9.1	318	61	152.1	±	3.4
Tiro4-30	233	101	0.43	0.04770	6.9	0.16300	8.0	0.02430	2.6	0.00790	6.1	0.330	-2	154.8	4.0	152.5	11.0	378	88	154.8	±	4.0
Tiro4-02	900	750	0.83	0.04980	4.0	0.16600	4.4	0.02444	2.1	0.00847	4.8	0.484	0	155.7	3.3	155.8	6.4	214	41	155.7	±	3.3
Tiro4-36	357	152	0.43	0.05110	5.9	0.17440	5.7	0.02451	2.0	0.00806	4.2	0.356	4	156.1	3.2	162.9	9.0	339	63	156.1	±	3.2
Tiro4-27	185	110	0.60	0.09530	6.2	0.34200	6.7	0.02493	2.6	0.01268	5.0	0.382	47	158.8	4.0	297.0	17.0	1587	83	158.8	±	4.0
Tiro4-38	97	42	0.44	0.06950	9.2	0.24600	10.2	0.02522	3.3	0.01040	8.7	0.324	27	160.6	5.3	221.0	20.0	980	120	160.6	±	5.3
Tiro4-35	334	143	0.43	0.05250	6.7	0.18100	6.6	0.02534	3.3	0.00975	6.7	0.494	5	161.3	5.2	170.1	10.0	433	77	161.3	±	5.2
Tiro4-06	498	474	0.95	0.05370	4.8	0.28400	5.3	0.03859	1.8	0.01195	2.8	0.339	4	244.1	4.3	254.6	12.0	385	54	244.1	±	4.3
Tiro4-17	166	181	1.09	0.07550	3.4	1.74000	4.4	0.16720	2.2	0.04988	2.8	0.507	2	996.0	20.0	1021.0	28.0	1088	40	996.0	±	20
Tiro4-19	348	55	0.16	0.08230	3.0	2.29800	3.8	0.20150	1.8	0.06390	3.3	0.485	2	1083.0	20.0	1210.0	27.0	1268	40	1183.0	±	20

n = 40   **Mean 206Pb/238U =   149.4   ± 1.2**
(2 sigma, MSWD = 2.0; n = 1)

^{a} U and Th concentrations (ppm) are calculated relative to analyses of trace-element glass standard NIST 610.

^{b} Isotopic ratios are corrected relative to 91500 standard zircon for mass bias and down-hole fractionation (91500 with an age ~1065 Ma; Wiedenbeck *et al.*, 1995). Isotopic 207Pb/206Pb ratios, ages and errors are calculated following Paton *et al.* (2010).

^{c} All errors in isotopic ratios are in percentage whereas ages are reported in absolute and given at the 2-sigma level. The weighted mean 206Pb/238U age is also reported in absolute values at the 2-sigma level. The uncertainties have been propagated following the methodology discussed by Paton *et al.* (2010).

^{d} Rho is the error correlation value for the isotopic ratios 206Pb/238U and 207Pb/235U calculated by dividing these two percentage errors. The Rho value is required for plotting Concordia diagrams. Percentage discordance values are obtained using the following equation (100*[(207Pb/235U age) – (206Pb/238U age)]/207Pb/235U age) proposed by Ludwig (2003). Positive and negative values indicate normal and inverse discordance, respectively.

^{e} Individual zircon ages in bold were used to calculate the weighted mean 206Pb/238U age and MSWD (Mean Square of Weighted Deviates) using the software program Isoplot (Ludwig, 2003).

criticized (*e.g.* Verma *et al.*, 2012). As an alternative, new discriminant-function based on multidimensional diagrams for basic–intermediate (Fig. 9) and acid (Fig. 10) rocks using Linear Discriminant Analysis (LDA) of natural logarithm ratios of major elements, immobile major and trace elements, and immobile trace elements were applied to discriminate MORB, Island Arc (IA), Continental Arc (CA), within-plate (CR: Continental Rift; OI: Ocean Island), and collisional (COL) settings.

Multidimensional discriminant diagrams have confirmed an affinity to subduction tectonic setting for intermediate rocks (Fig. 9; Agrawal *et al.*, 2004, 2008), although it is more likely an island arc rather than a continental arc setting. This distinction was simply not possible from conventional diagrams (Fig. 8A, B). In addition, the intermediate rocks included in the El Alamar Fm. show relatively high ratios of Th/Nb ~1.5 and La/Nb ~5 as observed in island arc systems (Fig. 11; Plank, 2005).

On the other hand, the sets of diagrams for felsic rocks (Fig. 10; Verma *et al.*, 2012) based on major and relatively immobile trace elements also show a subduction-related environment, but clearly a continental arc (rather than an island arc) setting was actually indicated. In addition, felsic volcanism included in the Minas Viejas Fm., as well as the observed in the La Boca Fm., display relatively restricted ratios of immobile elements (Th/Nb< 1.5; La/Nb< 5; Fig. 11; Plank, 2005). These geochemical features probably also imply that continental crust was involved in the petrogenesis process. U-Pb zircon geochronology data for the rhyodacite Tiro-4 has been reported in Table
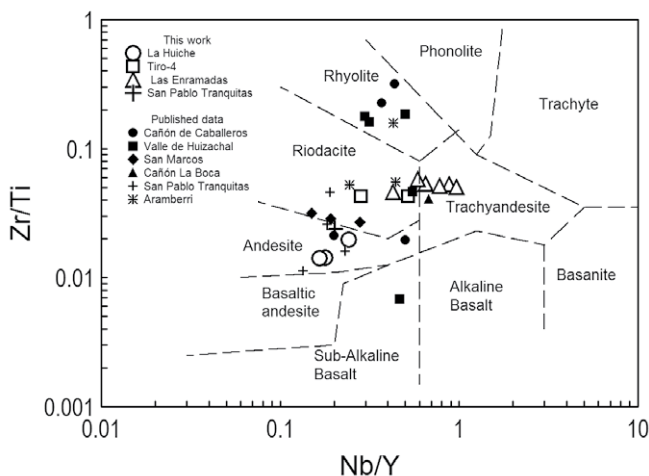
FIGURE 5. Zr/Ti - Nb/Y diagram (Winchester and Floyd, 1977) applied to Early Mesozoic volcanic rocks from Galeana (La Huiche, Tiro-4, San Pablo Tranquitas, and Las Enramadas) and published data (Bartolini *et al.,* 1999; Rubio-Cisneros, 2012; Barboza-Gudiño *et al.,* 2008): Valle de Huizachal, Cañón La Boca, Cañón Cabelleros, Arramberri, San Pablo Traquitas (see Figure 1).

3. Concordia diagrams and a weighted mean age plot have been displayed in the Fig. 12A-C, whereas the position of the LA-ICP-MS spots in selected zircon crystals has been reported in Figure 12D. These results have revealed that the activity of the Nazas continental arc may have reached up to 149.4 ± 1.2Ma (n= 21; MSWD= 2.0), as suggested by Stern and Dickinson (2010). Also, two Mesoproterozoic (1183 ± 20 and 996 ± 20Ma) and one Triassic (244 ± 4Ma) inherited grains have been detected in the sample Tiro-4.

Late Triassic–Jurassic geological framework for Northeastern Mexico

Subduction has been essential in the growth of Mexico. Mineralogic and geochemical data presented here suggest that, during the Late Triassic–Jurassic period, this phenomenon evolved from an island arc to a continental arc. However, what drove this change is not fully understood. We suggest the following tectonic scenario, based on a variant of the model proposed by Lee *et al.* (2007) for the North America Cordillera (Fig. 13):

i) Island arc/Late Triassic (Fig. 13A): Subduction of the Farallon plate (old cold oceanic lithosphere) beneath North America resulted in trench retreat and slab rollback, generating extension in the upper plate creating a fringing island arc. The El Alamar redbed fluvial system was deposited in extensional basins. A rifting event was in progress inboard of the Pangea continental margin (Goldhammer, 1999). Barboza-Gudiño *et al.* (2014) proposed 220Ma (Late Triassic) as a maximum depositional age for the El Alamar (Fig. 2). Petrographic and geochemical redbed features discard clastic contribution of the island arc system. The main source of the El Alamar Fm. was recycled material from Pangea continental crust. Andesitic dykes and sills (Fig. 5) emplaced in this unit display an island arc geochemical affinity (Figs. 9; 11). It is important to note that a distinction between island and continental arc was not established in previous literature for the El Alamar volcanism. This situation was due to an incomplete geochemical database and that the available diagrams did not have the ability to discriminate between these tectonic settings (Fig. 8). However, radiometric dating for the El Alamar basic to intermediate rocks is problematic, as amphibole and plagioclase phenocrysts are strongly altered (Fig. 4A, B) and zircon is scarce (Table 1). Nevertheless, some geological evidences can be useful to delimit the island arc period in the Northeastern Mexico. First, both siliciclastic and volcanic El Alamar rocks were affected by oblique-normal faulting (Fig. 3A), an event which does not appear to have affected La Joya deposits (Middle Jurassic; Fig. 2). In other areas (Valle de Huizachal; Rubio-Cisneros *et al.*, 2011) the overlying La
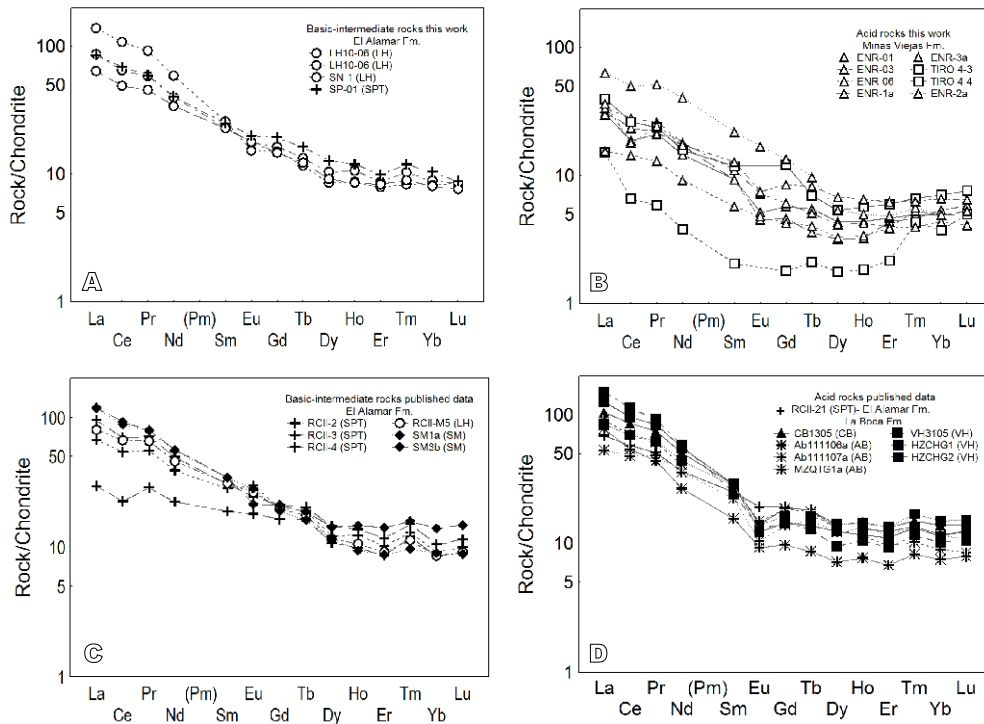
FIGURE 6. Chondrite-normalized REE diagrams for Galeana volcanic rocks. Normalization data (ppm) from Haskin *et al.* (1968) and Nakamura (1974): La= 0.329, Ce= 0.865, Pr= 0.112, Nd= 0.63, Sm= 0.203, Eu= 0.077, Gd= 0.276, Tb= 0.047, Dy= 0.343, Ho= 0.07, Er= 0.225, Tm= 0.03, Yb= 0.22, Lu= 0.0339. A) Basic-intermediate volcanism included in the El Alamar Fm.; B) Acid volcanism included in the Minas Viejas Fm.; C, D) Basic-Intermediate and acid volcanism included in the El Alamar and La Boca fms. (published data: Rubio-Cisneros, 2012; Barboza-Gudiño *et al.,* 2008). Localities: ENR: Las Enramadas, LH: La Huiche, SPT: San Pablo Tranquitas, SM: San Marcos, CB: Cañon La Boca, VH: Valle de Huizachal, AB: Aramberri.
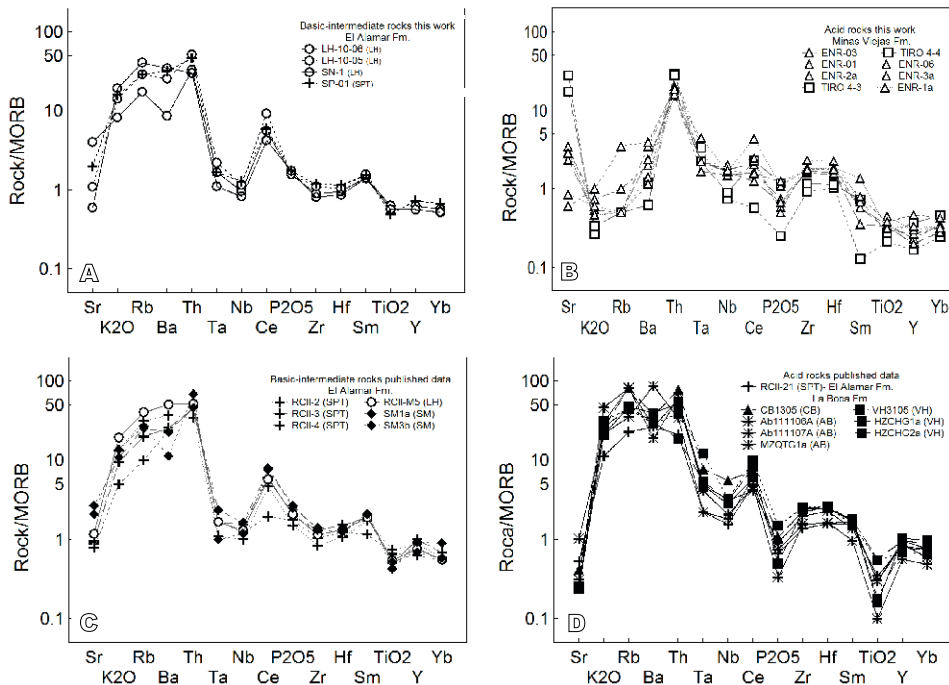
FIGURE 7. MORB-normalized multielemental diagrams for Galeana volcanic rocks. Normalization data (%wt, major elements; ppm, trace elements) from Pearce (1982): Sr= 120, K_2O= 0.15, Rb= 2, Ba= 20, Th= 0.20, Ta= 0.18, Nb= 3.5, Ce= 10, P_2O_5= 0.12, Zr= 90, Hf= 2.40, Sm= 3.3, TiO_2= 1.5, Y= 30, Yb= 3.4, Cr= 250. A) Basic-intermediate volcanism included in the El Alamar Fm.; B) Acid volcanism included in the Minas Viejas Fm.; C and D) Intermediate and acid volcanism included in the El Alamar and La Boca fms. (published data: Rubio-Cisneros, 2012; Barboza-Gudiño *et al.,* 2008). Symbols as in Figure 6.
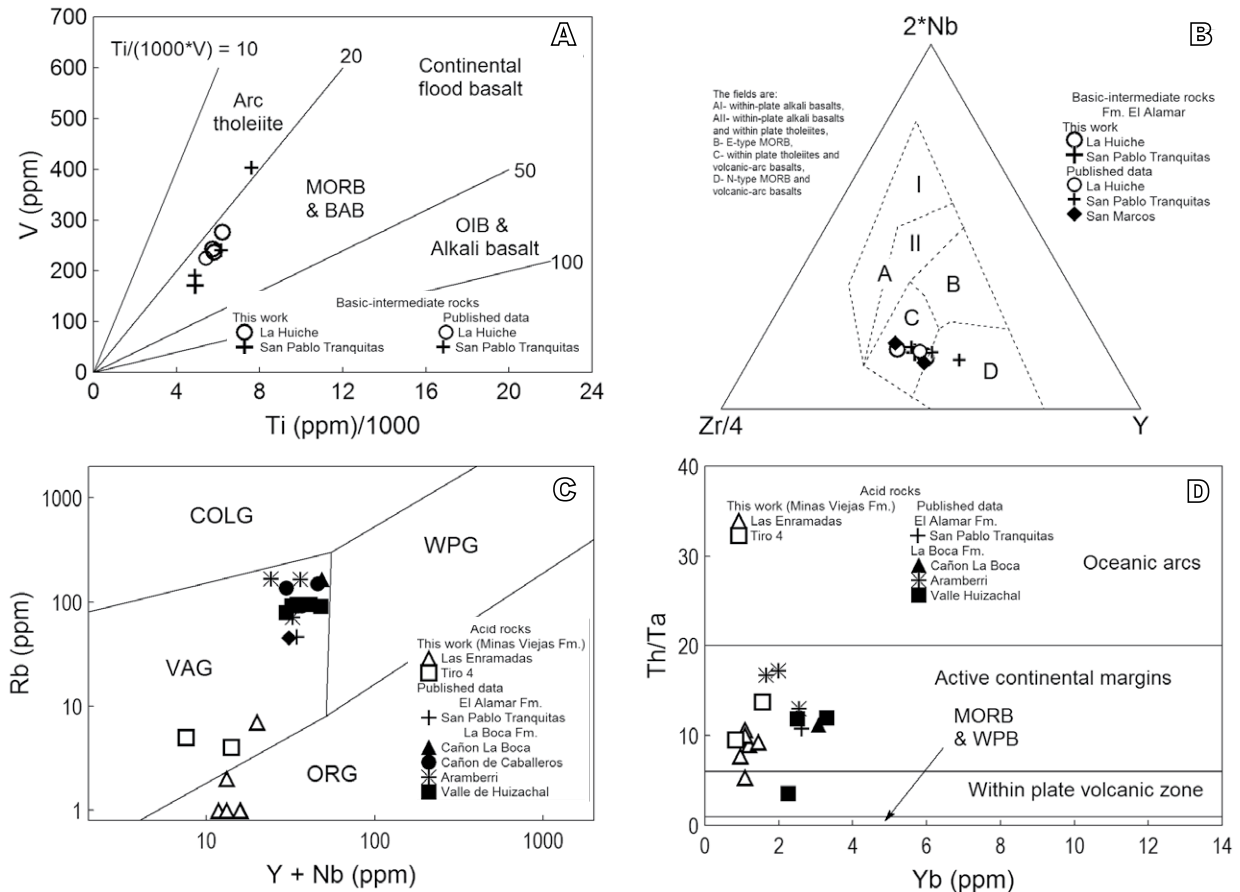
FIGURE 8. Tectonic discrimination diagrams for Early Mesozoic volcanic rocks from Galeana and other regions (Rubio-Cisneros, 2012; Barboza-Gudiño *et al.,* 2008). Basic-intermediate rocks: A) Ti – V (Shervais, 1982), B) Zr – Nb – Y (Meschede, 1986). Acid rocks: C) Rb – Y+Nb (Pearce *et al.,* 1984), D) Yb – Th/Ta (Gorton and Schandl, 2000). MORB: Mid-Ocean Ridge Basalt, BAB: Back Arc Basalts, COLG: collisional granite, VAG: Volcanic Arc Granite, ORG: Ocean Ridge Granite.

Boca Fm. also displays extensional faulting, that opened the spaces for the migration of mineralizing solutions and rhyolithic volcanism. In any case, the oblique-normal faulting is clearly post-El Alamar and pre-La Joya. Second, volcanic fragments included in the La Joya Fm., with a comparable texture and mineral arrangement to andesitic dykes and sills, have been observed in the San Pablo Tranquitas locality (Fig. 3D1, D2). Third, the oldest felsic volcanism reported in the La Boca Fm. has been dated in ~193Ma (Fig. 2). Thus, the island arc system could have developed after ~220Ma and before ~193Ma.

ii) Transitional regime/Early Jurassic (Fig. 13B): As the age of the subducting Farallon plate decreased, the plate tectonic setting evolved to a continental arc. However, Barboza-Gudiño *et al.* (2010) reported a sedimentation-volcanism hiatus during the Triassic (Rhaetian)–Jurassic (Hettangian) boundary. Later, the volcanic activity was reactivated and its acid products were emplaced in La Boca Fm. (Valle de Huizachal). U-Pb zircon geochronology reveals an age range of 189-193Ma for the volcanic rocks included in this unit (Fig. 2; Fastovsky *et al.*, 2005; Barboza-Gudiño *et al.*, 2008).

iii) Continental arc regime/Later Jurassic (Fig. 13C): With continuing continental crustal growth, a mature continental arc developed. In some locations, the redbed deposits were overlaid by the Minas Viejas Fm.; acid volcanism linked with this unit (Fig. 5), shows a continental arc affinity (Figs. 10; 11). Pyroclastic rocks dated by U-Pb zircon geochronology at 164.8Ma (Fig. 2; Cross, 2012). In the present work, applying the same method, the Tiro-4 dome was dated at 149.4 ± 1.2Ma (Fig. 12). Kroeger and Stinnesbeck (2003) also suggested that volcanism in Galeana was accompanied by local uplift and the stretching of the crust. However, these authors do not reported evidence of rift-related magmas.

Finally, long-lived fluctuations between icehouse and greenhouse states after Cambrian times have been linked to change from an island arc regime to a continental arc involving carbonate platforms (Lee *et al.*, 2013). It is important to note that, the island arc stage could represent a subduction event that occurred between the Permian-Triassic arc and the Nazas arc. Rhyodacitic to
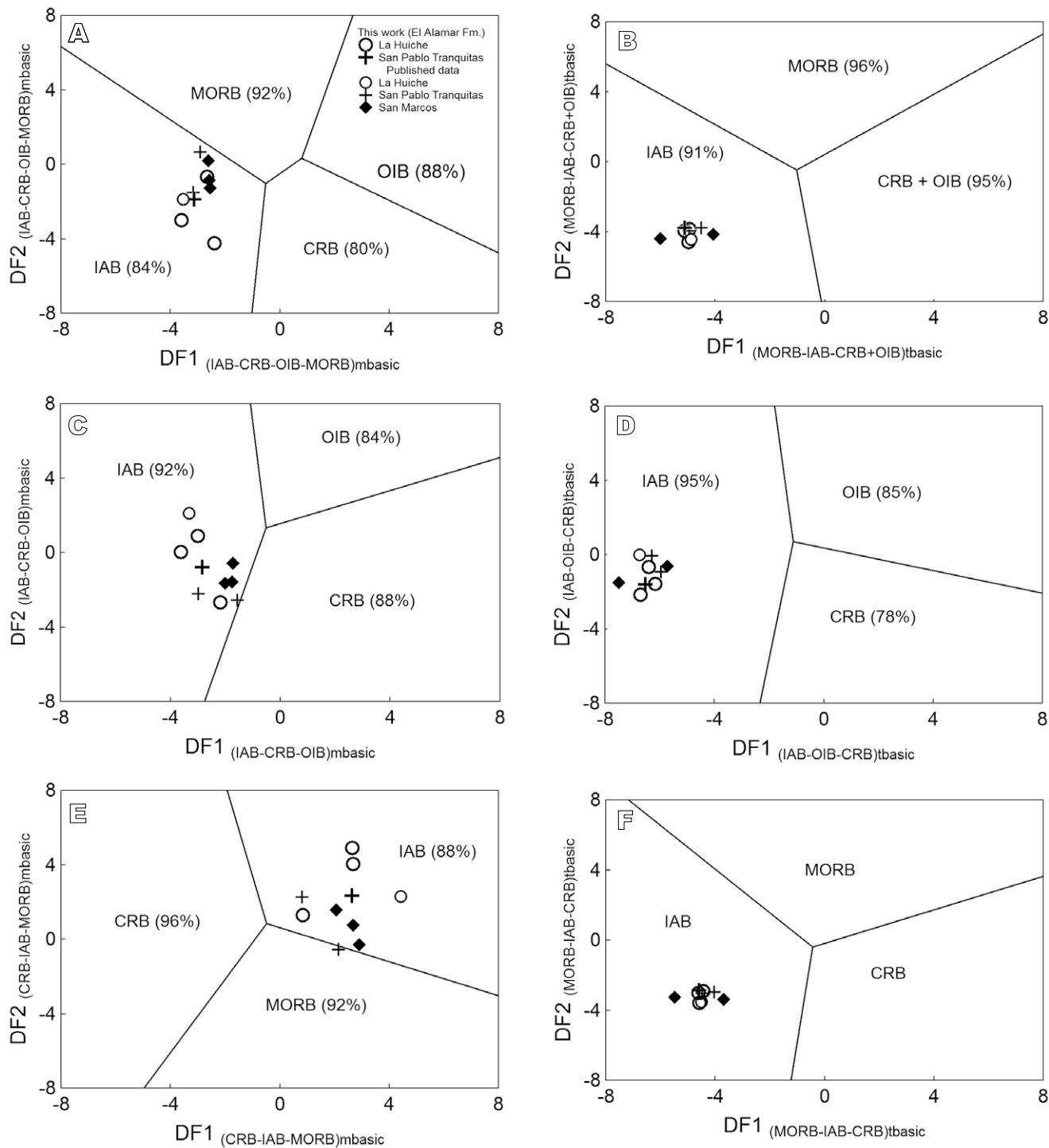
FIGURE 9. Multi-dimensional discriminant diagrams (Agrawal *et al.,* 2004, 2008; Major elements: A, C and E; Trace elements: B, D and F) applied to Early Mesozoic basic-intermediate rocks from Galeana and other areas (Rubio-Cisneros, 2012; Barboza-Gudiño *et al*., 2008). Tectonic settings: IAB: Island-Arc Basalt, CRB: Continental-Rift Basalt, OIB: Ocean-Island Basalt, MORB: Mid-Ocean Ridge Basalt.

rhyolithic domes (Tiro-4 and Las Enramadas) included in the Minas Viejas Fm. could be the last activity related to Nazas continental arc. Thus, barite mineralization in the Galeana area could be partly related to this Late Jurassic magmatism.

CONCLUSIONS

In the Galeana area of northeastern Mexico, scarce altered volcanic rocks are found in the siliciclastic El Alamar (Late Triassic) and evaporitic Minas Viejas (Middle to Late Jurassic) formations.
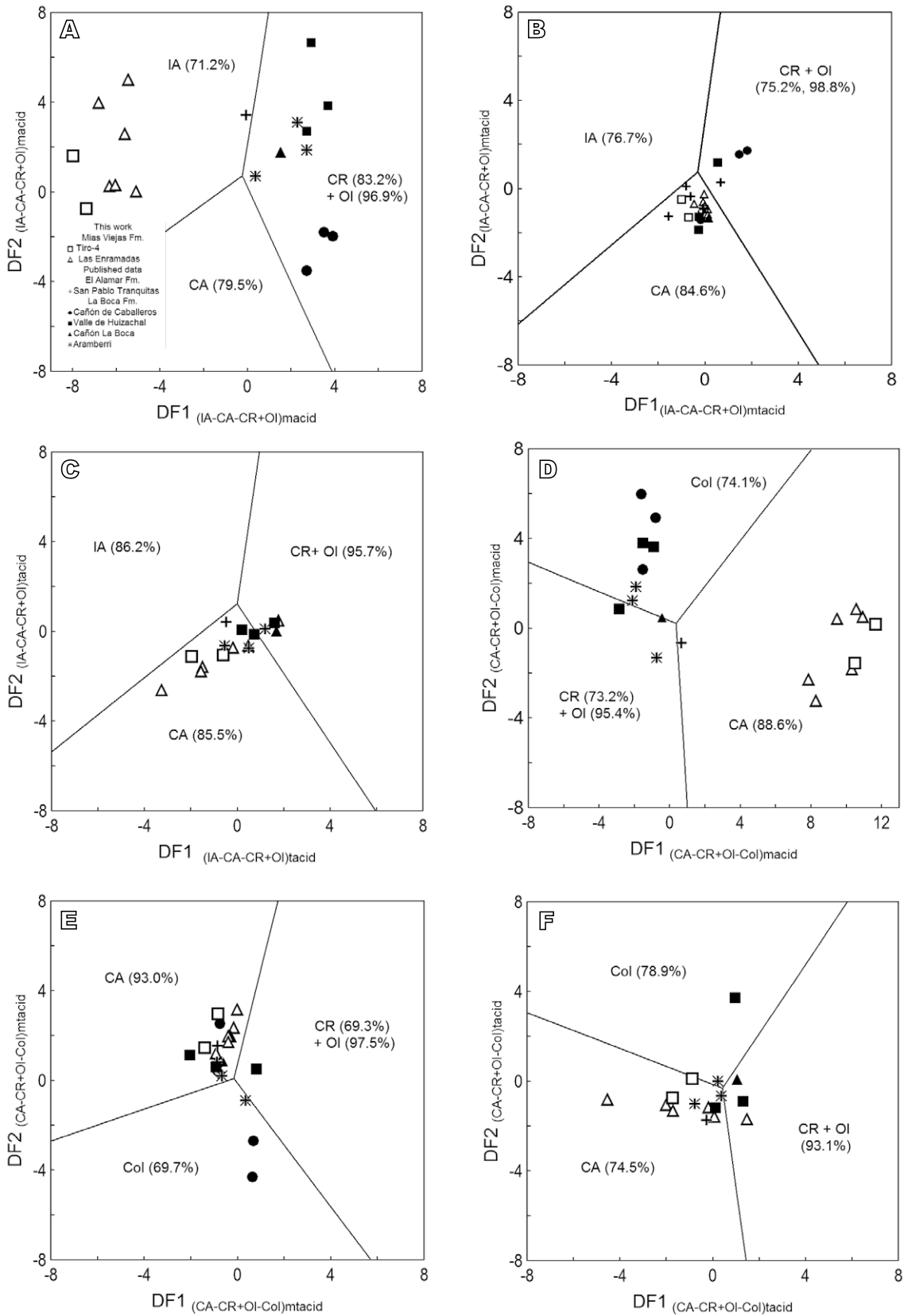
FIGURE 10. Multi-dimensional discriminant diagrams (Verma *et al.,* 2012; Major elements: A and D; Major/Trace elements: B and E; Trace elements: C and F) applied to Early Mesozoic acid rocks from Galeana and other areas (Rubio-Cisneros, 2012; Barboza-Gudiño *et al.,* 2008). Tectonic settings: IA: Island-Arc, CR: Continental-Rift, OI: Ocean-Island, CA: Continental Arc, Col: collision.

Andesitic dykes and sills included in siliciclastic rocks display a porphyritic texture with amphibole and plagioclase phenocrysts embedded in an aphanitic groundmass composed of altered glass and plagioclase microcrystals. Andesites have chondrite-normalized REE patterns characterized by light-REE enrichment, negative Eu anomaly absent, and a flat-pattern for heavy-REE. Multi-element MORB-normalized diagrams for these rocks are characterized by marked enrichments in LILE and small depletion of Nb-Ta and TiO_2. Conventional and statistical-based discriminant diagrams have revealed an island arc tectonic affinity. According to fieldwork and petrographic evidence, this island arc system developed after ~220Ma and before ~193Ma.

Rhyodacitic to trachyandesitic domes contained within evaporitic rocks show porphyritic to trachytic textures with plagioclase, K-feldspar, and quartz, embedded in a fine grained matrix of the same minerals and glass. These rocks display chondrite-normalized
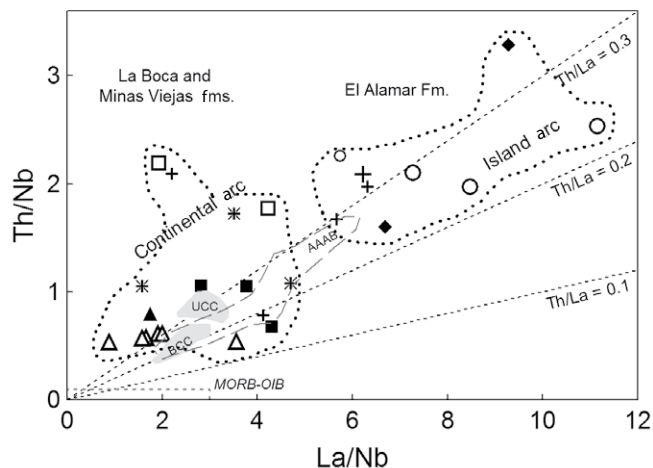
FIGURE 11. Th/Nb – La/Nb diagram (Plank, 2005) for Early Mesozoic volcanic rocks from Galeana and other areas (Rubio-Cisneros, 2012; Barboza-Gudiño *et al.*, 2008). Abbreviations: MORB: Mid-Ocean Ridge Basalts, OIB: Oceanic Island Basalts; UCC: Upper Continental Crust; BCC: Bulk Continental Crust; AAAB: Antilles and Aleutians Arc Basalts.
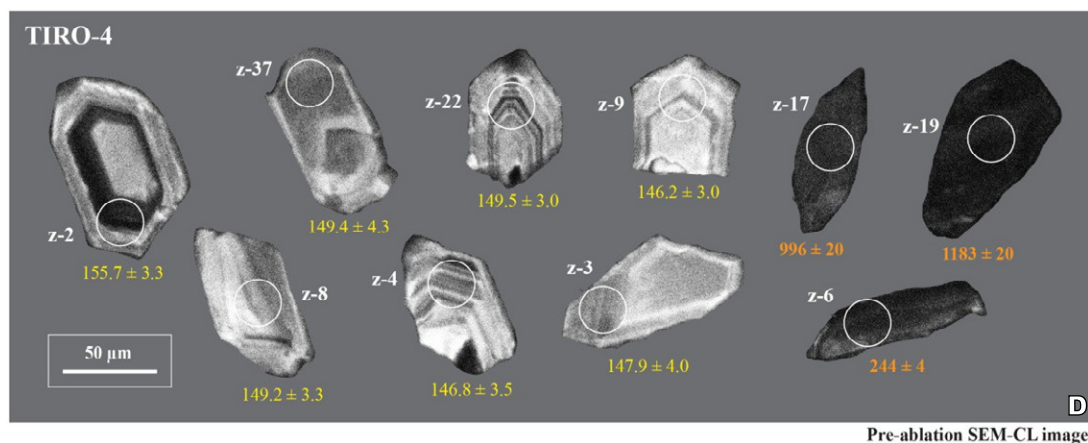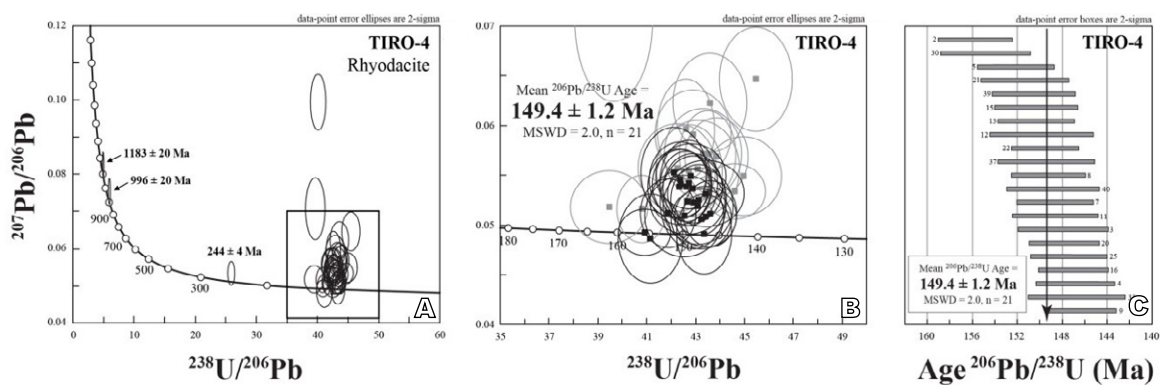
FIGURE 12. Tera–Wasserburg concordia diagrams (A and B) and weighted mean age plot (C) for rhyodacite sample TIRO-4. The most concordant U-Pb zircon analyses used for the $^{206}Pb/^{238}U$ age calculation (n = 21) are shown as black-line error ellipses with black squares in concordia diagrams (A and B) and as gray bars in weighted mean age plot (C). D) SEM-Cathodoluminiscence images of representative dated zircons from the rhyodacite sample TIRO-4; white circles and the adjacent numbers represent the spot size (~23μm) and the spot number, respectively. The $^{206}Pb/^{238}U$ ages are reported in Ma at the 2-sigma level of precision. Note there are some Proterozoic and Triassic xenocrystic zircon grains with darker CL colors in the rhyodacite sample.

REE patterns comparable to those showed by the andesitic rocks. However, the multi-element MORB-normalized diagrams show zig-zag patterns with lower concentration in lithophile elements. According to discriminant tectonic diagrams, they could be considered as continental arc magmas. U-Pb zircon geochronology data (this work and the literature) suggest that the arc system developed from ~193Ma to at least ~149Ma.

Late Triassic to Jurassic volcanic rocks of the northeastern Mexico sedimentary sequences are related to continental arc development along the North America western margin. However, considering new mineralogic, geochemical, and geochronologic data, and geological framework, we have identified a post 220Ma island arc system that evolved to a continental arc before ~193Ma. A three-step model has been suggested to explain the evolution of the development of an extensional basin, where redbeds and evaporites were contemporaneously deposited, linked to an arc system development: i) Late Triassic/island arc andesitic dykes and sills in the El Alamar Fm.; ii) Early Jurassic/continental rhyolitic flow and domes in the La Boca Fm. and iii) Late Jurassic/continental trachy-andesitic and rhyodacitic domes in the Minas Viejas Fm.
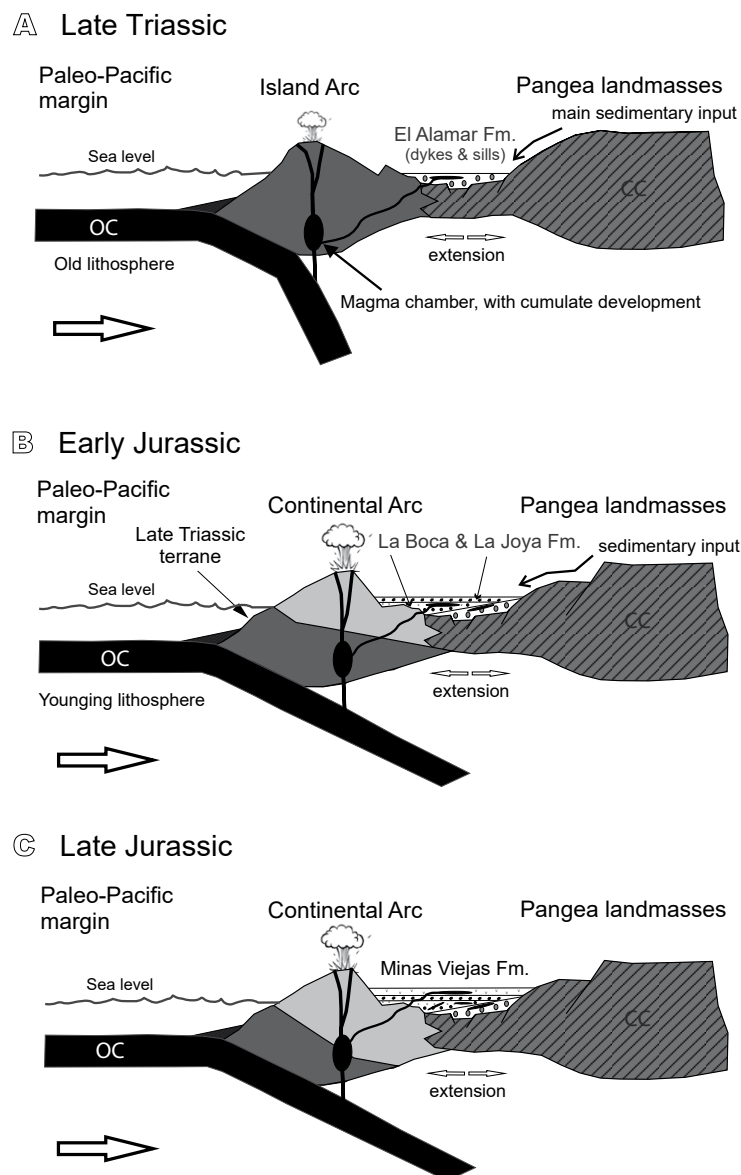
FIGURE 13. Three-step general scheme, based on the geochemical features and age of volcanism, as well as the tectonic framework, proposed to explain the Northeastern Mexico geological evolution during Late Triassic – Jurassic: A) Island arc regime/Late Triassic; B) Transitional regime/Early Jurassic and C) Continental arc regime/Late Jurassic. OC: Oceanic Crust, CC: Continental Crust.

ACKNOWLEDGMENTS

REFERENCES

Agrawal, S., Guevara, M., Verma, S.P., 2004. Discriminant analysis applied to establish major-element field boundaries for tectonic varieties of basic rocks. International Geology Review, 46, 575-594.

Agrawal, S., Guevara, M., Verma, S.P., 2008. Tectonic discrimination of basic and ultrabasic volcanic rocks through log-transformed ratios of immobile trace elements. International Geology Review, 50, 1057-1079.

Barboza-Gudiño, J.R., Tristán-González, M., Torres-Hernández, J.M., 2008. The Late Triassic-Early Jurassic active continental margin of western North America in northeastern Mexico. Geofísica Internacional, 37(4), 283-292.

Barboza-Gudiño, J.R., Zavala-Monsiváis, A., Venegas-Rodríguez, G., Barajas-Nigoche, L.D., 2010. Late Triassic stratigraphy and facies from northeastern Mexico: Tectonic setting and provenance. Geosphere, 6, 621-640.

Barboza-Gudiño, J.R., Ocampo-Díaz, Y.Z.E., Zavala-Monsiváis, A., López-Doncel, R.A., 2014. Procedencia como herramienta para la subdivisión estratigráfica del Mesozoico temprano en el noreste de México. Revista Mexicana de Ciencias Geológicas, 31, 303-324.

Bartolini, C., Lang, H., Stinnesbeck, W., 1999. Volcanic rocks outcrops in Nuevo Leon, Tamaulipas and San Luis Potosí, Mexico: Remmants of the Permian-Early Triassic magmatic arc? In: Bartolini, C., Wilson, J.L., Lawton, T.F. (eds.). Mesozoic sedimentary and tectonic history of North-Central Mexico. Geological Society of America Special Paper, 340, 347-356.

Cross, G.E., 2012. Evaporite deformation in the Sierra Madre Oriental, northeastern Mexico: Décollement kinematics in an evaporate-detached thin-skinned fold belt. Ph.D. Thesis. Graduate School, The University of Texas at Austin, 547pp.

Dalziel, I.W.D., Lawver, L.A., Murphy, J.B., 2000. Plumes, orogenesis, and supercontinental fragmentation. Earth and Planetary Science Letters, 178, 1-11.

Dickinson, W.R., Lawton, T.F., 2001. Carboniferous to Cretaceous assembly and fragmentation of Mexico. Geological Society of America Bulletin, 113, 1142-1160.

Fastovsky, D.E., Hermes, O.D., Strater, N.H., Bowring, S.A., Clark, J.M., Montellano, M., Hernández, R.R., 2005. Pre-Late Jurassic fossil-bearing volcanic and sedimentary red beds of Huizachal Canyon, Tamaulipas, Mexico. In: Anderson, T.H., Nourse, J.A., McKee, J.W., Steiner, M.B. (eds.). The Mojave-Sonora megashear hypothesis: Development, assessment and alternatives. Geological Society of America Special Paper, 393, 233-258.

Goldhammer, R.K., 1999. Mesozoic sequence stratigraphy and paleogeographic evolution of Northeast Mexico. In: Bartolini, C., Wilson, J.L., Lawton, T.F. (eds.). Mesozoic sedimentary and tectonic history of North-Central Mexico. Geological Society of America Special Paper, 340, 1-58.

González-León, C.M., Solari, L., Valencia-Moreno, M., Rascon-Heimplel, M.A., Solé, J., González-Becuar, E., Lozano-Santacruz, R., and Pérez-Arvizu, O., 2016. Late Cretaceous to early Eocene magmatic evolution of the Laramide arc in the Nacozari quadrangle, northeastern Sonora, Mexico and its regional implications. Ore Geology Reviews, 81(3), 1137-1157. DOI: http://dx.doi.org/10.1016/j.oregeorev.2016.07.020

Gorton, M.P., Schandl, E.S., 2000. From continents to island arcs: a geochemical index of tectonic setting for arc-related and within-plate felsic to intermediate volcanic rocks. Canadian Mineralogist, 38, 1065-1073.

Gurnis, M., 1988. Largescale mantle convection and the aggregation and dispersal of supercontinents. Nature, 332, 695-699.

Gutiérrez-Alonso, G., Fernández-Suárez, J., Weil, A.B., Murphy, J.B., Nance, R.D., Corfu, F., Johnston, S.T., 2008. Self-subduction of the Pangea global plate. Nature Geosciences, 1, 549-553.

Haskin, L.A., Haskin, M.A., Frey, F.A., Wildman, T.R., 1968. Relative and absolute terrestrial abundances of the rare earths. In: Ahrens, L.H. (ed.). Origin and distribution of the elements. Oxford, Pergamon, 889-911.

Iriondo, A., Arvizu, H.E., 2009. Permian (~275-258Ma) granitic magmatism in NW Sonora, Mexico: The missing link to a large continental arc event in SW North America. Dallas, 43rd Annual Meeting, South Central Section of Geological Society of America, Geological Society of America, abstracts with programs, 41, 35.

Jones, N.W., McKee, J.W., Anderson, T.H., Silver, L.T., 1995. Jurassic volcanic rocks in northeastern Mexico: A possible remnant of a Cordilleran magmatic arc. In: Jacques-Ayala, C., González-León, C.M., Roldán-Quintana, J. (eds.). Studies on the Mesozoic of Sonora and adjacent areas. Geological Society of America Special Paper, 301, 179-190.

Kroeger, K.F., Stinnesbeck, W., 2003. The Minas Viejas Formation (Oxfordian) in the área of Galeana, Northeastern Mexico: Significance and syndepositional volcanism and related barite genesis in the Sierra Madre Oriental. In: Bartolini, C., Buffler, R.T., Blickwede, J. (eds.). The Circum-Gulf of Mexico and the Caribbean: Hydrocarbon habitats, basin formation, and plate tectonics. American Association of Petroleum Geologists Memoir, 79, 515-528.

Lee, C.-T.A., Morton, D.M., Kistler, R.W., Baird, A.K., 2007. Petrology and tectonics of Phanerozoic continent formation: From island arcs to accretion and continental arc magmatism. Earth Planetary Science Letters, 263, 370-387.

Lee, C.-T.A., Shen, B., Slotnick, B.S., Liao, K., Dickens, G.R., Yokohama, Y., Lenardic, A., Dasgupta, R., Jellinek, M., Lackey, J.S., Schneider, T., Tice, M.M., 2013. Continental arc-island arc fluctuations, growth of crystal carbonates, and long-term climate change. Geosphere, 9, 21-36.

Ludwig, K.R., 2003. User´s Manual for Isoplot 3.00: A geochronological toolkit for Microsoft Excel. Berkeley, Berkeley Geochronology Center, 4 (Special Publication), 74pp.

Meschede, M., 1986. A method of discriminating between different types of mid-ocean ridge basalts and continental tholeiites with the Nb-Zr-Y diagram. Chemical Geology, 56, 207-216.

Nakamura, N., 1974. Determination of REE, Ba, Fe, Mg, Na and K in carbonaceous and ordinary chondrites. Geochimica et Cosmochimica Acta, 38, 757-775.

Padilla y Sánchez, R., 1985. Las estructuras de la curvatura de Monterrey, Estados de Coahuila, Nuevo León, Zacatecas y San Luis Potosí. Revista del Instituto de Geología, Universidad Nacional Autónoma de México (UNAM), 6, 1-20.

Paton, C., Woodhead, J.D., Hellstrom, J.C., Hergt, J.M., Greig, A., Maas, R., 2010. Improved laser ablation U-Pb zircon geochronology through robust downhole fractionation correction. Geochemistry, Geophysics, Geosystems, 11, QOAA06. DOI: 10.1029/2009GC002618

Paton, C., Hellstrom, J., Paul, B., Woodhead, J., Hergt, J., 2011. Iolite: Freeware for the visualization and processing of mass spectrometric data. Journal of Analytical Atomic Spectrometry, 26, 2508-2518.

Pearce, J.A., 1982. Trace element characteristics of lavas from destructive plate boundaries. In: Thorpe, R.S. (ed.). Andesites. Chichester, Wiley, 525-548.

Pearce, J., Harris, N., Tindle, A., 1984. Trace elements discrimination diagrams for the tectonic interpretation of granitic rocks. Journal of Petrology, 25, 956-983.

Petrus, J.A., Kamber, B.S., 2012. VizualAge: a novel approach to laser ablation ICP-MS U-Pb geochronology data reduction. Geostandards and Geoanalytical Research, 36, 247-270.

Pindell, J., Horn, G.B., 2014. Rapid outer marginal collapse at the rift to drift transition of passive margin evolution. Basin Research, 26, 701-725.

Plank, T., 2005. Constraints from Thorium/Lanthanum on sediment recycling at subduction zones and the evolution of the continents. Journal of Petrology, 46, 921-944.

Rubio-Cisneros, I.I., 2012. Provenance analysis of the El Alamar, La Boca and the La Joya Formations, Northeastern of Mexico (Upper Triassic–Middle Jurassic). Ph.D. thesis, Facultad de Ciencias de la Tierra, Universidad Autónoma de Nuevo León, México, 226pp.

Rubio-Cisneros, I.I., Ramírez-Fernández, J.A., García-Obregón, R., 2011. Análisis preliminar de procedencia de rocas clásticas jurásicas del Valle de Huizachal, Sierra Madre Oriental: Influencia del vulcanismo sinsedimentario y el basamento cristalino. Boletín de la Sociedad Geológica Mexicana, 63, 137-156.

Salvador, A., 1991. Triassic–Jurassic. In: Salvador, A. (ed.). The Gulf of Mexico Basin. Geological Society of America, The Geology of North America, J, 131-181.

Shervais, J.W., 1982. Ti-V plots and the petrogenesis of modern and ophiolitic lavas. Earth and Planetary Science Letters, 59, 101-118.

Slama, J., Kosler, J., Condon, D., Crowley, J., Gerdes, A., Hanchar, J., Hortswood, M.S.A., Morris, G.A., Nasdala, L., Norberg, N., Schaltegger, U., Schoene, B., Tubrett, M.N., Whitehouse, M.J., 2008. Plešovice zircon–a new natural reference material for U–Pb and Hf isotopic microanalysis. Chemical Geology, 249, 1-35.

Solari, L.A., Gómez-Tuena, A., Bernal, J.P., Pérez-Arvizu, O., Tanner, M., 2010. U-Pb zircon Geochronology with an integrated LA-ICP-MS microanalytical workstation: Achievements in precision and accuracy. Geostandards and Geoanalytical Research, 34, 5-18.

Stern, R.J., Dickinson, W.R., 2010. The Gulf of Mexico is a Jurassic backarc basin. Geosphere, 6, 739-754.

Torres, R., Ruiz, J., Patchett, P.J., Grajales, J.M., 1999. A Permo-Triassic continental arc in Eastern Mexico: Tectonic implications for reconstructions of southern North America. In: Bartolini, C., Wilson, J.L., Lawton, T.F. (eds.). Mesozoic sedimentary and tectonic history of north-central Mexico. Geological Society of America Special Paper, 340, 191-196.

Verma, S.K., Pandarinath, K., Verma, S.P., 2012. Statistical evaluation of tectonomagmatic discrimination diagrams for granitic rocks and proposal of new discriminant-function-based multi-dimensional diagrams for acid rocks. International Geology Review, 54, 325-347.

Whitney, D.L., Evans, B.W., 2010. Abbreviations for names of rock-forming minerals. American Mineralogist, 95, 185-187.

Wiedenbeck, M., Allé, P., Corfu, F., Griffin, W.L., Meier, M., Oberli, F., Von Quadt, A., Roddick, J.C., Speigel, W., 1995. Three natural zircon standards for U–Th–Pb, Lu–Hf, trace-element and REE analyses. Geostandards Newsletter, 19, 1-23.

Winchester, J.A., Floyd, P.A., 1977. Geochemical discrimination of different magma series and their differentiation products using immobile elements. Chemical Geology, 20, 325-34.